

Article

The Optimization of Nickel-Rich Cathode-Material Production on a Pilot Plant Scale

Agus Purwanto ^{1,*}, Muhammad Nur Ikhsanudin ², Putri Putih Puspa Asri ³, Afifah Salma Giasari ³, Miftakhul Hakam ², Cornelius Satria Yudha ⁴, Hendri Widiyandari ⁵, Endah Retno Dyartanti ¹, Arif Jumari ¹ and Adrian Nur ¹

¹ Chemical Engineering Department, Engineering Faculty, Universitas Sebelas Maret, Jl. Ir. Sutami No. 36, Surakarta 57126, Indonesia; endah_rd@staff.uns.ac.id (E.R.D.); arifjumari_ft@staff.uns.ac.id (A.J.); adriannur@staff.uns.ac.id (A.N.)

² Centre of Excellence for Electrical Energy Storage Technology, Universitas Sebelas Maret, Jl. Slamet Riyadi 435, Surakarta 57146, Indonesia; nurikhsanudin6798@gmail.com (M.N.I.); miftakhulhakam17@gmail.com (M.H.)

³ Business Development Department, PT VKTR, Teknologi Mobilitas, Bakrie Tower 35th Floor, Jl. H.R. Rasuna Said, Jakarta 12940, Indonesia; putri.asri@vktr.id (P.P.P.A.); afifah.giasari@vktr.id (A.S.G.)

⁴ Chemical Engineering Department, Vocational School, Universitas Sebelas Maret, Jl. Kolonel Sutarto 150 K, Surakarta 57126, Indonesia; corneliussyudha@staff.uns.ac.id

⁵ Department of Physics, Faculty of Mathematics and Natural Science, Universitas Sebelas Maret, Jl. Ir. Sutami 36 A, Surakarta 57126, Indonesia; hendriwidiyandari@staff.uns.ac.id

* Correspondence: aguspurwanto@staff.uns.ac.id

Abstract: Lithium-ion batteries (LIBs) remain the cornerstone of EV technology due to their exceptional energy density. The selection of cathode materials is a decisive factor in LIB technology, profoundly influencing performance, energy density, and lifespan. Among these materials, nickel-rich NCM cathodes have gained significant attention due to their high specific capacity and cost-effectiveness, making them a preferred choice for EV energy storage. However, the transition from the laboratory-scale to industrial-scale production of NMC-811 cathode material presents challenges, particularly in optimizing the oxidation process of Ni²⁺ ions. This paper addresses the challenges of transitioning NMC-811 cathode material production from a lab scale to a pilot scale, with its high nickel content requiring specialized oxidation processes. The important point emphasized in this transition process is how to produce cathode materials on a pilot scale, but show results equivalent to the laboratory scale. Several optimization variations are carried out, namely, the optimization of the heating rate and the calcination and sintering temperatures, as well as oxygen variations. These two aspects are important for large-scale production. This paper discusses strategies for successful pilot-scale production, laying the foundation for industrial-scale manufacturing. Additionally, NMC-811 cathodes are incorporated into 18650 cylindrical cells, advancing the adoption of high-performance cathode materials.

Keywords: electric vehicle; Li-ion battery; cathode; NMC-811; pilot scale



Citation: Purwanto, A.; Ikhsanudin, M.N.; Asri, P.P.P.; Giasari, A.S.; Hakam, M.; Yudha, C.S.; Widiyandari, H.; Dyartanti, E.R.; Jumari, A.; Nur, A. The Optimization of Nickel-Rich Cathode-Material Production on a Pilot Plant Scale. *Processes* **2024**, *12*, 685. <https://doi.org/10.3390/pr12040685>

Received: 2 February 2024

Revised: 23 March 2024

Accepted: 25 March 2024

Published: 28 March 2024



Copyright: © 2024 by the authors. Licensee MDPI, Basel, Switzerland. This article is an open access article distributed under the terms and conditions of the Creative Commons Attribution (CC BY) license (<https://creativecommons.org/licenses/by/4.0/>).

1. Introduction

The world is facing a climate crisis due to global warming, with a temperature increase of 2.7 °C, as reported by McKinsey Energy Insights Global Energy Perspective (2021) [1]. Industry, transportation, and other sectors contribute nearly 60% of CO₂ emissions from fossil fuel consumption. To reduce emissions and the burden of fuel subsidies, the government is promoting the use of Battery Electric Vehicles (BEVs) [2,3]. From 2012 to 2020, the global automotive landscape witnessed a remarkable transformation in the field of new energy vehicles (NEVs), including Battery Electric Vehicles (BEVs) and Plug-in Hybrid Electric Vehicles (PHEVs). During these eight years, NEV sales surged from 140,000 to 3.07 million units, representing an impressive annual compound growth rate of 47%, while market permeability climbed from 0.2% to 4% [2,4]. This growth was mainly due to global

energy-conservation and emission-reduction policies. Governments worldwide encourage NEV adoption through incentives and stricter emissions standards, aligning with efforts to combat climate change and air pollution. NEVs are set for rapid expansion, playing a vital role in sustainable transportation and environmental responsibility [5].

Given the need for high energy density, lithium-ion batteries (LIBs) are the predominant option for the batteries employed in electric vehicles [6]. Although there have been suggestions and developments in post-lithium technologies like solid-state batteries (SSBs), sodium-ion batteries, lithium–sulfur batteries, lithium–air batteries, and multivalent batteries, these alternatives have not yet matured technologically compared to state-of-the-art LIBs. As a result, it is most likely that LIBs will continue to maintain their market dominance for at least the next decade [7,8].

The choice of cathode material remains a critical factor in LIB technology that significantly impacts the advancement and broader adoption of LIBs [9]. Cathodes play a pivotal role in determining the overall performance, energy density, and lifespan of LIBs [10]. Numerous cathode materials have undergone investigation to enhance the energy density of LIBs. Among these cathode materials, nickel-rich NCM cathodes have garnered significant research attention for high-energy applications owing to their greater specific capacity. The higher mass proportion of nickel also reduces the cobalt content, contributing to a relatively low cost [11,12]. Currently, electric vehicle (EV) manufacturers, including VW, GM, Tesla, BYD, BAIC, Nissan, and Hyundai, are either in the process of planning or have already adopted NCM-811 (or its variations such as NCMA-811 with a small amount of aluminum) as their advanced cathode chemistry [13,14]. Achieving a specific capacity of $220 \text{ mA}\cdot\text{h g}^{-1}$ is possible through elevated nickel (Ni) contents and higher charging voltages. This level of capacity is immensely coveted for the forthcoming generation of electric vehicles (EVs). Manufacturers are targeting ranges over 600 km per charge, bringing them near the ranges of internal-combustion-engine vehicles [13,15,16]. This advancement is particularly significant considering the desire for longer driving distances and the transition towards more sustainable transportation options.

So far, several factors have influenced the success of the production transition from the laboratory scale to the industrial scale. NMC-811 has a high nickel content and can be classified as a nickel-rich cathode. This requires special treatment, especially in the heating process, to ensure that the oxidation of the Ni^{2+} ions contained in the precursor can take place optimally. This study utilized oxalate-based coprecipitation, as this method does not necessitate an inert atmosphere and is more environmentally friendly. In the oxalate coprecipitation method, the valence state of manganese always remains divalent and stable in an aqueous environment. Oxalate-based coprecipitation can produce fine-sized NMC with excellent homogeneity [17]. The hydroxide coprecipitation process uses sodium hydroxide (NaOH) and requires ammonia (NH_3) as a chelating agent. In this process, the chelating agent (NH_3) is needed in large quantities. Precipitation waste containing NH_3 is dangerous for operators if inhaled and pollutes water ecosystems, so it is not environmentally friendly if applied on an industrial scale. Oxalate coprecipitation, which does not require inert conditions, is also an advantage because Co ions are oxidized when the reaction process is carried out inertly [18]. In terms of increasing the production scale, the coprecipitation method with oxalate is easier to carry out compared to methods using other precipitate agents. Apart from being environmentally friendly, oxalic acid is a cheap material, which is one of the main considerations for its use in industrial-scale NMC cathode production. Therefore, this paper aims to discuss optimization and steps concerning pilot-scale NMC-811 production, which will be the initial basis for moving to an industrial scale. The correlation between the morphology and crystallinity of NMC-811 and the electrochemical performance of fabricated batteries with 18650 cylindrical cells using cathode NMC-811 are carefully analyzed.

2. Materials and Methods

2.1. Materials

The main materials used in this production were nickel sulfate hexahydrate ($\text{NiSO}_4 \cdot 6\text{H}_2\text{O}$) from Zenith, Taichung, Taiwan; manganese sulfate monohydrate ($\text{MnSO}_4 \cdot \text{H}_2\text{O}$) from China; cobalt sulfate heptahydrate ($\text{CoSO}_4 \cdot 7\text{H}_2\text{O}$) from Rubamin, Gujarat, India; and lithium hydroxide monohydrate ($\text{LiOH} \cdot \text{H}_2\text{O}$) from Yujiang Chemical, China. The supporting materials used were oxalic acid dihydrate ($\text{H}_2\text{C}_2\text{O}_4 \cdot 2\text{H}_2\text{O}$) from Jinan, China, as a precipitation agent, and sodium hydroxide (NaOH) from Asahimas Chemical, Ltd., Jakarta, Indonesia, as a pH control. For Li-ion battery fabrication, powdered cathode and anode materials needed to be coated on the surface of the current collector. Before coating, NMC-811 and graphite cathode powders (Gelon, Linyi, China) were made in slurry form to facilitate coating. The conductive agent acetylene black (Gelon, China) was added to the slurry, and binders with a mixture of carboxymethyl cellulose (CMC) (Yucmc, Hebi, China) and styrene butadiene rubber (SBR) (Gelon, China) with water were used as a solvent. The anode was battery-grade graphite (Gelon, China). The current collector for the cathode was aluminum foil, and the current collector for the anode was copper foil from Gelon, China.

2.2. Methodology

2.2.1. Material Production

The precursor was prepared with an acidic process by mixing $\text{NiSO}_4 \cdot 6\text{H}_2\text{O}$, $\text{MnSO}_4 \cdot \text{H}_2\text{O}$, and $\text{CoSO}_4 \cdot 7\text{H}_2\text{O}$ in distilled water with a Ni:Mn:Co molar ratio of 8:1:1 for the TM (transition metal) source. The TM mixture solution was added to a 1 M oxalic acid solution in a reactor, and a greenish colloidal solution was obtained. Then, 5 M NaOH was added as a pH adjuster to obtain a pH of 3, and the mixing solution was heated at 65 °C for 2 h. After the mixing process took place, the precipitation solution was washed using water. The washing process was carried out four times using the sedimentation and draining method to reach pH 7. The precipitate that formed was dried in an oven overnight to remove the water content, and a dry powder formed called an NMC811–oxalate precursor (NMC811-OX).

The NMC811–oxalate precursor was mixed with lithium hydroxide ($\text{LiOH} \cdot \text{H}_2\text{O}$) in the solid state. The solid mixture was calcinated and sintered in various temperature conditions under oxygen gas flow. In the laboratory-scale production, a maximum of only 500 g of NMC cathode products can be made. The production scheme carried out on a pilot scale was planned to produce with a base capacity of 10 kgs of NMC-811 cathode products for the entire production line from the raw-material mixing process to the heating process in the furnace. Two variations of muffle furnaces were used in these materials' development:

1. Furnace-K (MTI, Model KSL-1200X-UL) had a heating chamber volume of 30 cm × 20 cm × 12 cm (W × D × H) and reached temperatures up to 1200 °C;
2. Furnace-B had a heating chamber volume of 60 cm × 60 cm × 60 cm (W × D × H) and reached temperatures up to 1200 °C (Zhengzhou Protech Technology Co., Ltd., Model BS-A1200-216L, Zhengzhou, China).

2.2.2. Material Characterization

Basic material testing was carried out on the NMC811 cathode to analyze the quality of the product before it was fabricated in the form of a Li-ion battery. Fourier-Transform Infrared Spectroscopy (FTIR) was used to analyze the hydrocarbon functional groups in the NMC-811 cathode sample using a Shimadzu FTIR tool from Kyoto, Japan. Crystallinity analysis was carried out on the NMC-811 cathode with a Bruker D8 Advance X-Ray Diffractometer (XRD) from Ettlingen, Germany. Thermal tests were also carried out on precursor NMC (p-CAM) samples to identify changes in mass during the heating process. This test used a Thermogravimetric Analysis (TGA) product from Shimadzu, Kyoto, Japan. Scanning Electron Microscopy (SEM) was carried out on cathode samples to determine the morphological appearance of the material and evaluate the uniformity of particle

shapes and sizes. The SEM tool used in this case was a JEOL Benchtop JCM-7000 from Tokyo, Japan.

2.2.3. Electrochemical Performance of Li-Ion Batteries

In LIBs, cell production consists of three main steps: electrode manufacture, cell assembly, and cell finishing. The cells contained an NMC-811 cathode, a graphite anode, a polyethylene separator, and an electrolyte (LiPF₆). The first step was manufacturing the electrode. The cathode slurry was formed using water-based and room-temperature conditions. A slurry consisting of NMC-811 powder, acetylene black, CMC, and SBR was dissolved in distilled water as a solvent. Mixing the cathode slurry was an important part of obtaining a better dispersion of powder material in the polymer matrix [19]. In addition, the anode slurry was prepared by mixing graphite, acetylene black, CMC, and SBR in distilled water. After the slurry was ready, the cathode NMC-811 was coated in conductive foil and an aluminum roll and the anode graphite slurry was coated in a copper roll. The process of coating the conductive foil was continuously transferred to the dryer. The dried electrode sheet was pressed using a rotary pressing machine and then cut with an electrode width of 5.6 cm. Then, the cathode NMC-811, polyethylene separator, and anode graphite were prepared automatically for the 18650 cylindrical cells. The negative-to-positive ratio (*n/p* ratio) for the anode and cathode was 1.2. The mass loading on the cathode sheet was 33.5 mg/cm² and the mass loading on the anode sheet was 15.81 mg/cm². The cells were aged for a night to remove any water components under atmospheric pressure and a temperature of 60 °C. After the aging stage, 5 mL of a 1 M LiPF₆ electrolyte was added to the cells, and the cells were closed and sealed for the formation analysis. The electrochemical performance test of the NMC-811 cathode material was carried out by making it into a 18650 Li-ion battery. This test was carried out with a Neware 8 Channel Battery Analyzer (Xiamen, China) with a voltage window of 2.5–4.3 Volts at a current of 0.05 C. This test is called a formation test.

3. Results and Discussion

3.1. Characterization of NMC811

The Scanning Electron Microscopy (SEM) analysis aimed to analyze the cathode's particle size, surface morphology, and uniformity. Figure 1 shows images of the results of morphological tests on NMC-811 cathode samples with two magnification variations: 500× and 5000×. Based on the SEM test results, the particle size was uniform and there was no significant agglomeration between the particles. At a sufficient magnification with a scale of 5 μm, it could be seen that the primary particles gathered together to form secondary particles. A commercial cathode material has a particle size in the range of 1–25 μm, with an average size of around 10.5 μm, and a dense spherical particle shape [3,12,20].

Meanwhile, the shape of the cathode material produced with both the small furnace (FK) and large furnace (FB) was not as good as that of the commercial NMC-811 cathode material but could be classified as pebbles that were close to spherical [12,20]. Managing the particle size within the active phase is crucial because the rate capability of a battery is closely connected to the diffusion path length of the charge species. The FK cathode material exhibited a broad particle-size distribution spanning from 9 to 63 μm, with an average size of 25.4 μm. This characteristic was indicative of its inherent heterogeneity. The FB group cathode produced secondary particles with irregular shapes and heterogeneous characteristics. The size distribution was wide, varying from 2 to 22 μm with an average size of 7.53 μm for FB-1, from 9 to 32 μm with an average size of 9.8 μm for FB-2, and from 9 to 50 μm with an average size of 20.3 μm for FB-3. The FK featured a small-volume chamber that supported excellent heat and gas flow distribution, resulting in a dense pebble-like structure closely resembling a spherical shape [3,21].

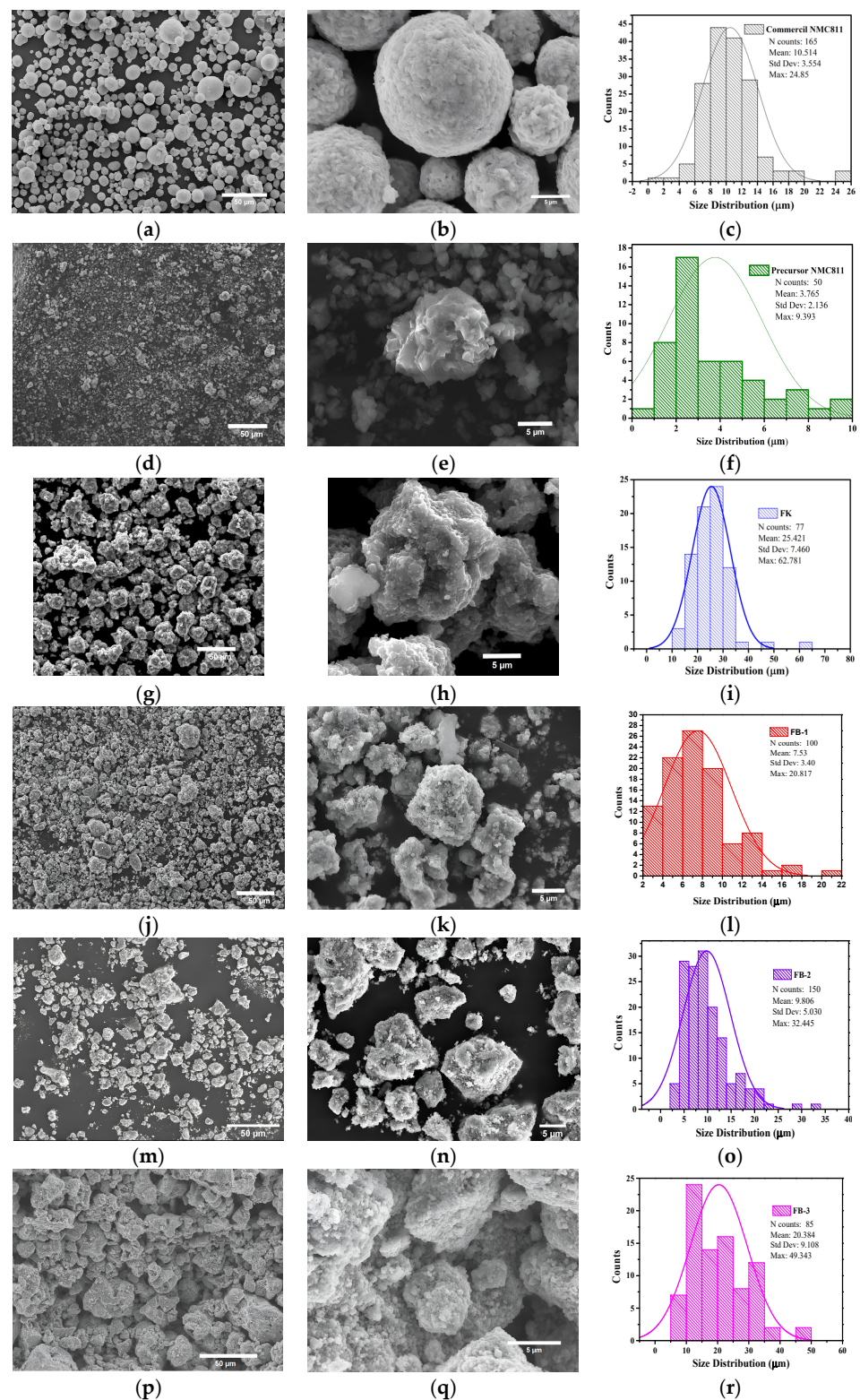


Figure 1. Morphology analysis of NMC-811 cathode material. (a–c) SEM images at 500 \times and 2500 \times magnification and particle-size distribution of commercial NMC811. (d–f) SEM images at 500 \times and 2500 \times and particle-size distribution of NMC-oxalate precursor. (g–i) SEM images at 500 \times and 2500 \times and particle-size distribution of NMC-811 produced with small furnace (FK). (j–l) SEM images at 500 \times and 2500 \times and particle-size distribution of NMC-811 produced with large furnace with process condition 1 (FB-1). (m–o) SEM images at 500 \times and 2500 \times and particle-size distribution of NMC 811 FB with process condition 2 (FB-2). (p–r) SEM images at 500 \times and 2500 \times and particle-size distribution of NMC-811 FB with process condition 3 (FB-3).

In contrast, the FB had a chamber volume approximately 30 times greater than the FK's. Consequently, it is more likely that the heat distribution in the FB was not as effective as in the FK, leading to a more irregular structure in the morphology of the FB-group cathode materials. The process conditions were adjusted considering the larger chamber in the FB (Table 1). The holding times in the calcination and sintering processes were extended, and the gas flow was increased by three or four times compared to the FK, aiming to support a more efficient oxidation process. Despite these modified process conditions, the current conditions were still inadequate for producing cathode materials with a desirable morphology.

Table 1. Variations in the heating rate and O₂ flow rate during the heating process.

Muffle Furnace	Variation Code	Process Condition									O ₂ Flow Rate L/min
		Calcination			Sintering			Cooling			
		T ₁ (°C)	HT* (min)	T ₀ (°C)	Time (min)	T ₁ (°C)	HT* (min)	T ₀ (°C)	Time (min)	T ₁ (°C)	
Furnace-K	FK	450	360	450	70	800	900	800	180	30	5
	FB-1	450	360	450	100	800	900	800	250	30	15
Furnace-B	FB-2	450	480	450	100	800	1020	800	250	30	15
	FB-3	450	480	450	100	800	1140	800	250	30	20

* HT = Holding time.

FTIR was applied to investigate the surface chemical composition of the NMC-811-oxalate precursor and the active material NMC-811 before and after the sintering stage, as shown in Figure 2. Before sintering, the NMC-oxalate precursor and the NMC-811 MA displayed significant peaks at 3346 cm⁻¹, 1611 cm⁻¹, and 1312 cm⁻¹, which, respectively, represented O-H, C=O, and C-O bonds from the carboxyl functional group of oxalic acid. The oxidation process was successfully achieved in both the FK and FB materials after the sintering process, as indicated by the disappearance of organic functional groups in the FTIR spectra of both materials. C-O bond peaks vanished at about 1400–1300 cm⁻¹ for the FK and FB materials because of the dissociation of carboxyl in the heating process and the release of CO₂ gas.

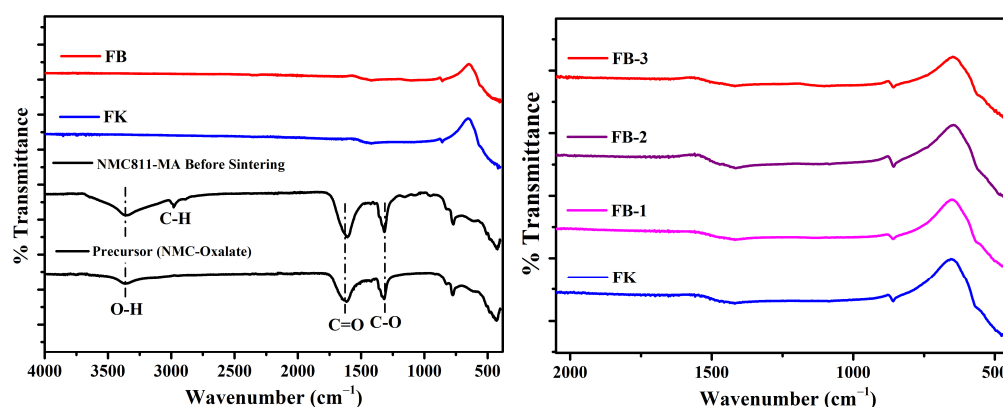
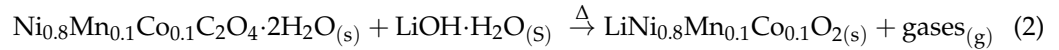
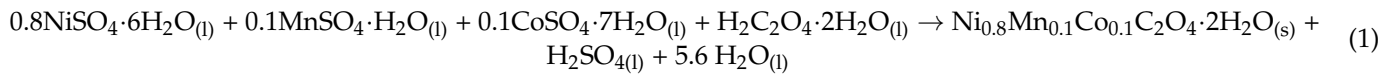


Figure 2. FTIR spectra of NMC-811 materials.

The peaks detected at 860 cm⁻¹ in NMC oxide for the FB and FK samples can be attributed to the existence of Li₂CO₃ impurities. These impurities arose from surface reactions between Li⁺ ions and atmospheric gases [1]. Despite successfully completing the oxidation reaction for both materials, obtaining a layered structure remained a critical objective. The FTIR results of the NMC-oxalate precursor and the NMC-811 active materials (FK-FB) were comparable to those of the reactions given in Equations (1) and (2):



XRD characterization was performed to determine the crystalline structures of NMC-811. Figure 3 presents the XRD patterns of the FK and FB samples. The XRD experimental data were compared to the Joint Committee on Powder Diffraction Standards (JCPDS) reference pattern No. 98-001-0448 using Highs Core Plus Software. The analysis identified that the diffraction pattern was compatible with the JCPDS No. 98-001-0448 of NMC. All peaks were indexed on the basis of the hexagonal α -NaFeO₂ structure with the R3m space group [2]. The well-ordered, layered material could be assessed utilizing the lattice parameter and the I ratio presented in Table 2. The substantiation of the layered configuration was established using the c/a ratio of the lattice parameter, which served as a direct indicator of the lattice's deviation from a perfect cubic close-packed lattice. An ideal close-packed lattice is characterized by a c/a value of 4.899 [4]. Notably, the observed c/a ratios in all our samples surpassed 4.900, affirming the presence of a well-organized layered structure. However, the doublet peaks for the (006)/(102) reflections at 37° (2θ) and the (018)/(110) reflections at 65° (2θ) were also indicative of the presence of ordered hexagonal layered structures [3]. The doublet peaks were obviously observed in FK and FB-3, while FB-1 and FB-2 did not show distinct splitting for the (006)/(102) and (018)/(110) reflections. This clearly confirmed that the longer heating time and the higher gas flow for the cathode material production with FB favored the formation of the well-ordered layered structure necessary for the efficient intercalation/deintercalation of lithium ions during battery charge–discharge cycles. This was evidenced by the clear peak splitting of the (006)/(102) and (018)/(110) reflections. Furthermore, the potential for cation mixing arose from introducing a small quantity of Ni²⁺ at the Li⁺ site. This mixing occurred because of the presence of Ni²⁺ during phase formation, detrimentally affecting the performance of the NMC cathode material. Replacing Li⁺ with Ni²⁺ obstructed the Li-ion pathway, leading to suboptimal electrochemical performance. It is noteworthy that a higher value of I(003)/I(104) corresponded to reduced cation mixing in the material [22]. The ideal value of I(003)/I(104) is >1.2. Table 2 indicates that the I(003)/I(104) ratio value was greater than 1.2 for all samples, signifying a low degree of cation mixing.

Table 2. Lattice parameter and I ratio of NMC sample.

No.	Materials	Heat Treatment Condition			a (Å)	c (Å)	c/a	I Ratio
		1st Step	2nd Step	O ₂ Flow (L/min)				
1	FK	450 °C, 360 min	800 °C, 15 h	5	2.881	14.230	4.939	1.505
2	FB-1	450 °C, 360 min	800 °C, 15 h	15	2.886	14.227	4.929	1.550
3	FB-2	450 °C, 480 min	800 °C, 17 h	15	2.887	14.203	4.919	1.734
4	FB-3	450 °C, 480 min	800 °C, 19 h	20	2.887	14.216	4.923	1.291

Thermogravimetric analysis (TGA) aims to analyze mass changes with a simulated increase in temperature according to the sintering temperature. Figure 4 displays the TGA test results of precursor NMC (p-CAM). The initial mass reduction, occurring in the temperature range of 100–150 °C, had a notable decrease of 8.04%. This reduction was attributed to the evaporation process, specifically the release of H₂O molecules trapped within the molecular structure. The second stage began in the temperature range of 150–200 °C and signified a subsequent decrease of 4.27%, which was associated with processes such as dehydration or hydrate release. A significant weight loss of 33.33%

was observed in the third stage in the temperature range of 200–500 °C, indicating the occurrence of NMC–oxalate decomposition to NMC oxide [23]. The reactions in these processes are shown in Equations (1) and (2). These findings were consistent with those of the FTIR test, which were noticeable due to the disappearance of organic functional groups in the FTIR spectra of both FK and FB materials. The disappearance of peaks was related to the breakdown of oxalate carboxyl groups during the heating process, leading to the release of CO₂ gas [24].

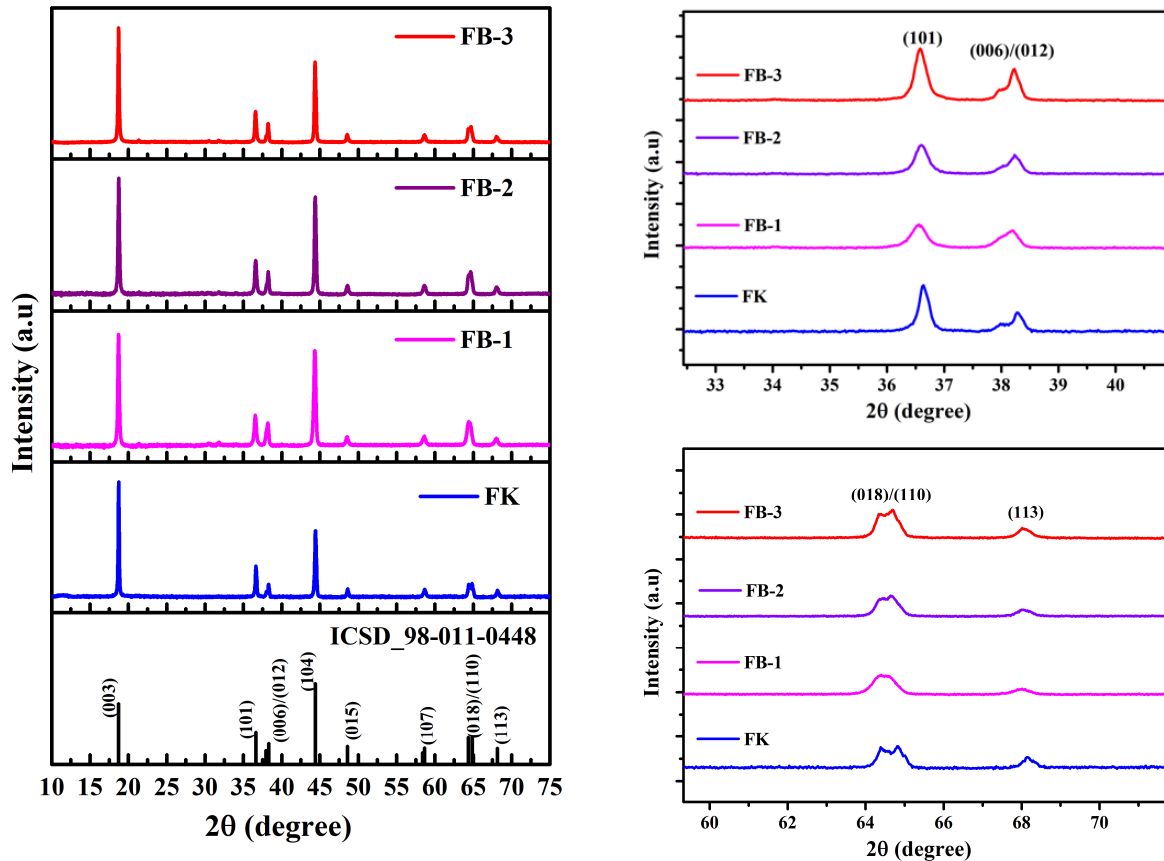


Figure 3. XRD analysis of NMC-811 from small furnace (FK) and large furnace (FB).

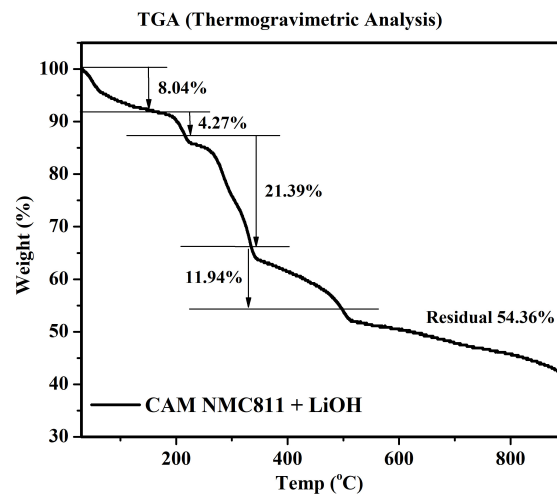


Figure 4. Thermogravimetric analysis (TGA) of NMC-811 cathode material.

3.2. Electrochemical Performance Analysis of NMC-811–Graphite Battery

The electrochemical performance test aimed to analyze the capabilities of the cathode material when fabricated in the form of a full-cell battery with a graphite anode. Graphite is an anode material that is widely used and is commonly used in the LIB industry. There are several alternative anode material choices, such as Hard Carbon [25]. However, due to its cheap price and fairly good performance when combined with LIB cathodes, in this experiment, graphite material was chosen as the anode. Electrochemical tests were carried out using cylindrical cell type 18650. The cylindrical type was chosen. It has good mechanical stability because it uses stainless steel for the outer case [26] and has wide applications for stationary energy-storage systems and moving vehicles such as e-bikes, e-motorcycles, and electric cars [26]. The produced NMC-811 cathode samples were evaluated for capacity based on commercial materials in this test. Figure 5a displays the battery capacity testing (discharge) results in the first cycle formation process with a current of 0.05 C. The commercial material showed a specific capacity result of 155 mA·h/g, and the produced cathode material showed specific capacity results of 115 mA·h/g (FB) and 154 mA·h/g (FK). The battery cell with the best performance-specific charge–discharge capacity was the one with NMC-811 synthesized in a small muffle furnace (FK) rather than FB. Based on the active material characterization, the crystallinity of NMC-811 in FK is superior to that in FB.

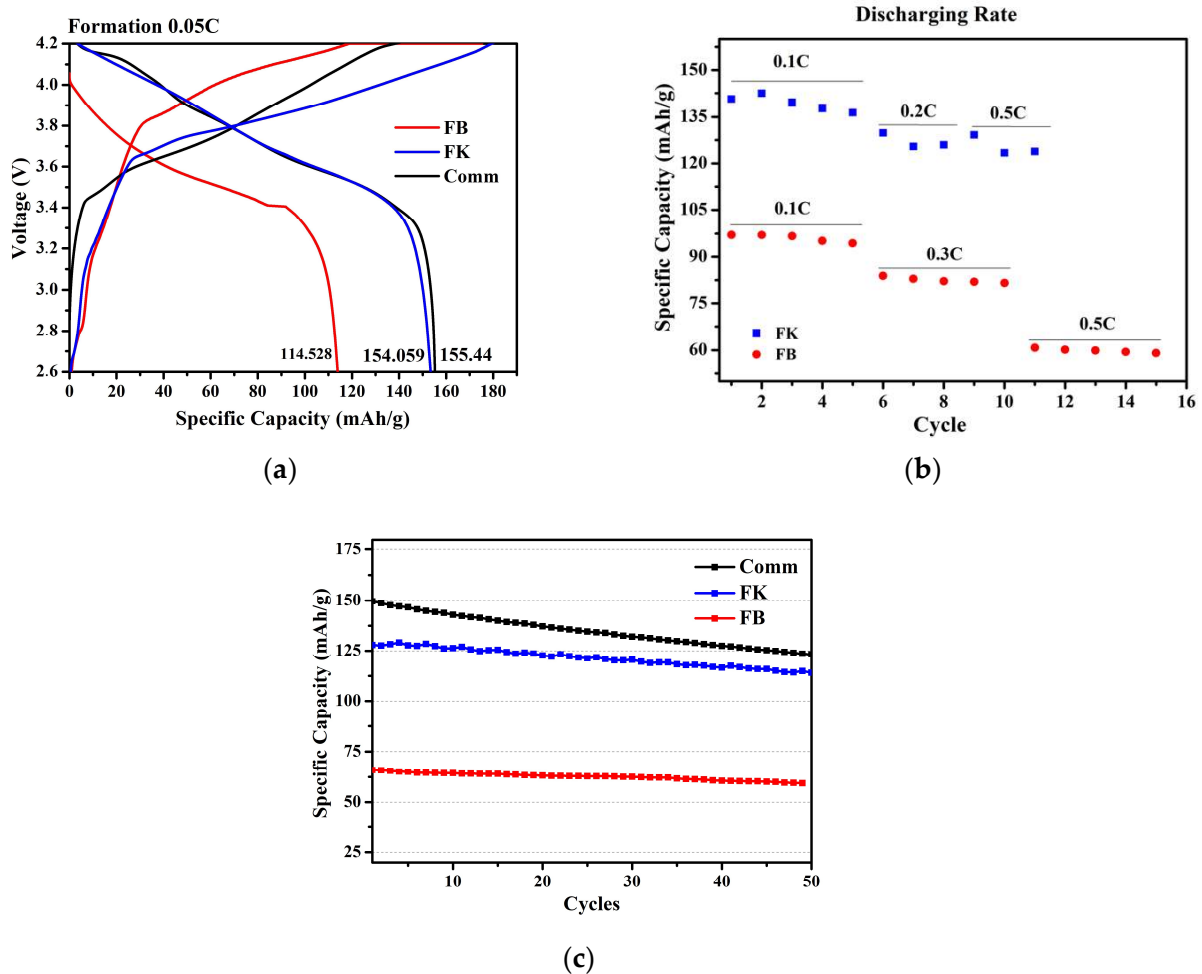


Figure 5. Electrochemical performance test results: (a) Full-cell analysis charge–discharge test at 0.05 C, (b) rate performance of NMC-811 cathode material, and (c) cycle stability at 0.5 C.

This result is considered quite useful because it shows that the capacity produced by FK batteries makes up 90% of the capacity of commercial materials assembled in the

same conditions. Apart from that, the durability of the battery was also tested at various currents. This rate-capability test used currents of 0.1, 0.2, and 0.5 C. The test results showed a decrease in capacity. The capacity decreased by 7.6% from 141 mA·h/g to 130 mA·h/g with a current of 0.2 C. Then, a decrease of 1.0% occurred from a current of 0.2 C to a current of 0.5 C. The rate-ability test is shown in Figure 5b.

The cycling performance of the FK and FB samples was compared with the commercial material for 50 cycles at 0.5 C, as shown in Figure 5c. Overall, the sample had excellent stability, although the specific capacity differed. At 0.5 C, the FK sample had a higher specific capacity than the FB sample, but the FB sample had good stability. It was concluded that the crystals of FB materials can still be considered to improve the specific capacity.

Table 3 confirms that extending the heating time and increasing the gas flow rate during large-scale production using FB improved the initial discharge capacity of the materials. Specifically, the measured values for FK, FB-1, FB-2, and FB-3 were 154 mA·h/g, 61 mA·h/g, 103 mA·h/g, and 114 mA·h/g, respectively. The cell-performance distribution was assessed using discharge data from 10 battery samples, and a narrower distribution was observed in the FB samples, as indicated by the low standard deviation. However, when compared to FK, a relatively low capacity was exhibited by FB. This was assumed to be due to the uneven distribution of oxygen gas in larger furnaces, as it may not be possible to attain the same level of uniformity observed in smaller-scale furnaces, thereby affecting the efficiency of the metal-oxidation process. The I ratio of FB in Table 2 indicates better cation mixing, but there are other factors that influenced the battery-capacity test results. Based on the SEM test results in Figure 1, it can be seen that the morphology of the FK and FB cathodes was rougher than that of the commercial materials. This resulted in the surface area of the material becoming larger, as the smaller the particle size, the greater the surface area. The average particle size data also show that the particle size of NMC-FB was smaller than that of commercial NMC. This also supports the existence of a larger Cathode Electrolyte Interface (CEI) phenomenon, thus indicating a large production material capacity compared to commercial NMC materials.

Table 3. Electrochemical performance and cell-performance distributions for FK and FB samples.

Cathode Material	Heat-Treatment Condition			Initial Discharge Capacity (mA·h/g) 0.05 C	Cell-Performance Distribution 0.05 C (N = 10)			
	First Step	Second Step	O ₂ Flow (L/min)		Min. (mA·h/g)	Max. (mA·h/g)	Mean (mA·h/g)	S·Dev
FK	450 °C, 360 min	800 °C, 15 h	5	154	134	154	141	6.91
FB-1	450 °C, 360 min	800 °C, 15 h	15	61	76	61	64	4.39
FB-2	450 °C, 480 min	800 °C, 17 h	15	103	98	104	101	2.21
FB-3	450 °C, 480 min	800 °C, 19 h	20	114	104	114	109	3.44

4. Conclusions

In conclusion, the successful pilot-scale production of the NMC-811 cathode material marks a significant milestone, paving the way for potential mass production. The thorough examination of NMC-811 cathode morphology revealed distinct characteristics among different cathode materials. While the commercial cathode material demonstrated a well-defined size and shape, the FK and FB cathode materials exhibited wider size distributions and pebble-like morphologies. Despite concerted efforts to improve the process conditions, particularly in the larger-volume FB chamber, challenges persist in achieving the intended cathode material morphology. This highlights the complexity of controlling particle size to enhance the battery's rate capability and the need for further refinement in the manufacturing process. Crystallography characterization further elucidated the sensitivity of NMC-811 crystallinity to the duration of sintering and calcination. The optimal crystallinity for the FB cathode material was achieved through 8 h of calcination and 19 h of sintering. This understanding is crucial, as it impacts the electrochemical performance of the battery. The electrochemical analysis comparing FK and FB revealed

promising results. With its optimized crystallinity, the FB cathode material could perform with an I ratio greater than 1.2, indicating reduced cation mixing. Regarding capacity, FB delivered 154 mA·h/g, outperforming FK at 115 mA·h/g across various performance rates. Moreover, stability was observed at different C rates (0.1 C, 0.2 C, and 0.5 C), suggesting greater performance. While these findings are encouraging, there is a recognized need for further research to fine-tune and optimize the electrochemical performance of the battery. This ongoing investigation aims to bridge the gap between the achieved capacity and the theoretical capacity of NMC-811, ultimately enhancing the practical viability of this cathode material for advanced energy-storage applications.

Author Contributions: Conceptualization, A.P. and C.S.Y.; methodology, M.N.I.; data curation and validation, P.P.P.A., A.S.G. and M.H.; writing—review and editing, P.P.P.A., A.S.G. and M.N.I.; visualization, H.W. and A.J.; supervision, E.R.D. and A.N. All authors have read and agreed to the published version of the manuscript.

Funding: This research was financially supported by The Directorate General of Higher Education, Research, and Technology (DGHERT) of the Ministry of Education, Culture, Research, and Technology (MOECRT) of the Republic of Indonesia through the Kedaireka program (project titled “The Utilization of Nickel as a Basic Material for Electric Vehicles”) with the Project ID 191.6/UN27.26/HK.07.00/2023 in collaboration with PT VKTR Teknologi Mobilitas company under Memorandum of Understanding (MoU) number 41.1/UN27.48/HK.07/2022249/PKS/VKTR/BOD/11-2022.

Data Availability Statement: The datasets generated and/or analyzed during the current study are available from the corresponding author on reasonable request.

Acknowledgments: This research was supported by a UNS collaboration with PT VKTR Teknologi Mobilitas through the Kedaireka program with MoU number 191.6/UN27.26/HK.07.00/2023.

Conflicts of Interest: Agus Purwanto, Arif Jumari, Endah Retno Dyartanti, and Adrian Nur are working as lecturers in the Chemical Engineering Department, Engineering Faculty, Universitas Sebelas Maret. Cornelius Satria Yudha is a lecturer in the Chemical Engineering Department, Vocational School, Universitas Sebelas Maret. Hendri Widiyandari is a lecturer in the Department of Physics, Faculty of Mathematics and Natural Science, Universitas Sebelas Maret. Muhammad Nur Ikhsanudin works in material production at the Centre of Excellence for Electrical Energy Storage Technology, Universitas Sebelas Maret. Putri Putih Puspa Asri and Afifah Salma Giasari work on RnD Battery Material Teams in the Business Development Department, PT VKTR, Teknologi Mobilitas.

References

1. McKinsey & Company. *Global Energy Perspective 2021*; McKinsey & Company: Chicago, IL, USA, 2021; p. 9.
2. Lv, Y.; Huang, S.; Zhao, Y.; Roy, S.; Lu, X.; Hou, Y.; Zhang, J. A review of nickel-rich layered oxide cathodes: Synthetic strategies, structural characteristics, failure mechanism, improvement approaches and prospects. *Appl. Energy* **2022**, *305*, 117849. [[CrossRef](#)]
3. Tiozzo, A.; Ghaseminezhad, K.; Mazzucco, A.; Giuliano, M.; Rocca, R.; Dotoli, M.; Nicol, G.; Nervi, C.; Baricco, M.; Sgroi, M.F. Investigating the Influence of Three Different Atmospheric Conditions during the Synthesis Process of NMC811 Cathode Material. *Crystals* **2024**, *14*, 137. [[CrossRef](#)]
4. Salgado, R.M.; Danzi, F.; Oliveira, J.E.; El-Azab, A.; Camanho, P.P.; Braga, M.H. The latest trends in electric vehicles batteries. *Molecules* **2021**, *26*, 188. [[CrossRef](#)]
5. Zhao, X.; Li, H.; Han, F.; Dai, M.; Sun, Y.; Song, Z.; Han, D.; Niu, L. Electrochemical exfoliation of graphene as an anode material for ultra-long cycle lithium ion batteries. *J. Phys. Chem. Solids* **2020**, *139*, 109301. [[CrossRef](#)]
6. Liu, Y.; Zhang, R.; Wang, J.; Wang, Y. Current and future lithium-ion battery manufacturing. *iScience* **2021**, *24*, 102332. [[CrossRef](#)]
7. Liu, W.; Placke, T.; Chau, K. Overview of batteries and battery management for electric vehicles. *Energy Rep.* **2022**, *8*, 4058–4084. [[CrossRef](#)]
8. Zhang, M.; Shen, J.; Li, J.; Zhang, D.; Yan, Y.; Huang, Y.; Li, Z. Effect of micron sized particle on the electrochemical properties of nickel-rich $\text{LiNi}_{0.8}\text{Co}_{0.1}\text{Mn}_{0.1}\text{O}_2$ cathode materials. *Ceram. Int.* **2019**, *46*, 4643–4651. [[CrossRef](#)]
9. Li, H.; Zhang, B.; Wu, Y.; Hou, J.; Jiang, D.; Duan, Q. Hydrogenated borophene/blue phosphorene: A novel two-dimensional donor-acceptor heterostructure with shrunken interlayer distance as a potential anode material for Li/Na ion batteries. *J. Phys. Chem. Solids* **2021**, *155*, 110108. [[CrossRef](#)]
10. Sim, S.-J.; Lee, S.-H.; Jin, B.-S.; Kim, H.-S. Use of carbon coating on $\text{LiNi}_{0.8}\text{Co}_{0.1}\text{Mn}_{0.1}\text{O}_2$ cathode material for enhanced performances of lithium-ion batteries. *Sci. Rep.* **2020**, *10*, 11114. [[CrossRef](#)]

11. Wijareni, A.S.; Widiyandari, H.; Purwanto, A.; Arif, A.F.; Mubarak, M.Z. Morphology and Particle Size of a Synthesized NMC 811 Cathode Precursor with Mixed Hydroxide Precipitate and Nickel Sulfate as Nickel Sources and Comparison of Their Electrochemical Performances in an NMC 811 Lithium-Ion Battery. *Energies* **2022**, *15*, 5794. [[CrossRef](#)]
12. Thao, L.T.; Van Truong, P.; Van Bo, N.; Son, L.T.; Van Tuan, N.; Phat, D.T.; Dat, N.Q.; Van Ky, N.; Lan, N.T.; Van Nguyen, T. Augmenting electrochemical performance of nickel-rich NMC for lithium-ion batteries by combining material synthesis modification and redistribution of transition metal ion concentration. *J. Phys. Chem. Solids* **2023**, *183*, 111616. [[CrossRef](#)]
13. Li, W.; Liu, X.; Xie, Q.; You, Y.; Chi, M.; Manthiram, A. Long-Term Cyclability of NCM-811 at High Voltages in Lithium-Ion Batteries: An In-Depth Diagnostic Study. *Chem. Mater.* **2020**, *32*, 7796–7804. [[CrossRef](#)]
14. Schmuch, R.; Wagner, R.; Hörpel, G.; Placke, T.; Winter, M. Performance and cost of materials for lithium-based rechargeable automotive batteries. *Nat. Energy* **2018**, *3*, 267–278. [[CrossRef](#)]
15. Li, W.; Erickson, E.M.; Manthiram, A. High-nickel layered oxide cathodes for lithium-based automotive batteries. *Nat. Energy* **2020**, *5*, 26–34. [[CrossRef](#)]
16. Zaghib, K.; Dontigny, M.; Guerfi, A.; Charest, P.; Rodrigues, I.; Mauger, A.; Julien, C. Safe and fast-charging Li-ion battery with long shelf life for power applications. *J. Power Sources* **2011**, *196*, 3949–3954. [[CrossRef](#)]
17. Yao, X.; Xu, Z.; Yao, Z.; Cheng, W.; Gao, H.; Zhao, Q.; Li, J.; Zhou, A. Oxalate co-precipitation synthesis of $\text{LiNi}_{0.6}\text{Co}_{0.2}\text{Mn}_{0.2}\text{O}_2$ for low-cost and high-energy lithium-ion batteries. *Mater. Today Commun.* **2019**, *19*, 262–270. [[CrossRef](#)]
18. Seo, J.-S.; Lee, J.-W. Fast growth of the precursor particles of $\text{Li}(\text{Ni}_{0.8}\text{Co}_{0.16}\text{Al}_{0.04})\text{O}_2$ via a carbonate co-precipitation route and its electrochemical performance. *J. Alloys Compd.* **2017**, *694*, 703–709. [[CrossRef](#)]
19. Jo, M.; Ku, H.; Park, S.; Song, J.; Kwon, K. Effects of Residual Lithium in the precursors of $\text{Li}[\text{Ni}_{1/3}\text{Co}_{1/3}\text{Mn}_{1/3}]\text{O}_2$ on their lithium-ion battery performance. *J. Phys. Chem. Solids* **2018**, *118*, 47–52. [[CrossRef](#)]
20. Wang, H.; Lin, J.; Zhang, X.; Wang, L.; Yang, J.; Fan, E.; Wu, F.; Chen, R.; Li, L. Improved Electrochemical Performance of $\text{LiNi}_{0.8}\text{Co}_{0.1}\text{Mn}_{0.1}\text{O}_2$ Cathode Materials Induced by a Facile Polymer Coating for Lithium-Ion Batteries. *Appl. Energy Mater.* **2021**, *4*, 6205–6213. [[CrossRef](#)]
21. Hawley, W.B.; Li, M.; Li, J. Room-Temperature Eutectic Synthesis for Upcycling of Cathode Materials. *Batteries* **2023**, *9*, 498. [[CrossRef](#)]
22. Setyawati, R.B.; Stulasti, K.N.R.; Azinuddin, Y.R.; Suci, W.G.; Aliwarga, H.K.; Dyartanti, E.R.; Purwanto, A. High power and thermal-stable of graphene modified $\text{LiNi}_{0.8}\text{Mn}_{0.1}\text{Co}_{0.1}\text{O}_2$ cathode by simple method for fast charging-enable lithium ion battery. *Results Eng.* **2024**, *21*, 101651. [[CrossRef](#)]
23. Nisa, S.S.; Rahmawati, M.; Yudha, C.S.; Nilasary, H.; Nursukatmo, H.; Oktaviano, H.S.; Muzayanha, S.U.; Purwanto, A. Fast Approach to Obtain Layered Transition-Metal Cathode Material for Rechargeable Batteries. *Batteries* **2022**, *8*, 4. [[CrossRef](#)]
24. Jia, H.; Dirican, M.; Aksu, C.; Sun, N.; Chen, C.; Zhu, J.; Zhu, P.; Yan, C.; Li, Y.; Ge, Y.; et al. Carbon-enhanced centrifugally-spun SnSb/carbon microfiber composite as advanced anode material for sodium-ion battery. *J. Colloid Interface Sci.* **2019**, *536*, 655–663. [[CrossRef](#)] [[PubMed](#)]
25. Wilke, C.; Kaas, A.; Peuker, U.A. Influence of the Cell Type on the Physical Processes of the Mechanical Recycling of Automotive Lithium-Ion Batteries. *Metals* **2023**, *13*, 1901. [[CrossRef](#)]
26. Ohneseit, S.; Finster, P.; Floras, C.; Lubenau, N.; Uhlmann, N.; Seifert, H.J.; Ziebert, C. Thermal and Mechanical Safety Assessment of Type 21700 Lithium-Ion Batteries with NMC, NCA and LFP Cathodes—Investigation of Cell Abuse by Means of Accelerating Rate Calorimetry (ARC). *Batteries* **2023**, *9*, 237. [[CrossRef](#)]

Disclaimer/Publisher’s Note: The statements, opinions and data contained in all publications are solely those of the individual author(s) and contributor(s) and not of MDPI and/or the editor(s). MDPI and/or the editor(s) disclaim responsibility for any injury to people or property resulting from any ideas, methods, instructions or products referred to in the content.